arXiv:1406.4713v1 [physics.atm-clus] 18 Jun 2014

Desorption Dynamics of Heavy Alkali Metal Atoms (Rb, Cs) off the Surface of Helium Nanodroplets

J. von Vangerow,[†] A. Sieg,[†] F. Stienkemeier,[†] M. Mudrich,[*,†] A. Leal,[‡] D. Mateo,[‡,¶] A. Hernando,[§] M. Barranco,[‡] and M. Pi[‡]

Physikalisches Institut, Universität Freiburg, 79104 Freiburg, Germany, Departament ECM, Facultat de Física and IN^{2}UB, Universitat de Barcelona, 08028 Barcelona, Spain, Department of Chemistry and Biochemistry, California State University at Northridge, 18111 Nordhoff St., Northridge, CA 91330, USA, and Laboratoire de Chimie Physique Moléculaire, Swiss Federal Institute of Technology Lausanne (EPFL), 1015 Lausanne, Switzerland

E-mail: mudrich@physik.uni-freiburg.de

Abstract

We present a combined ion imaging and density functional theory study of the dynamics of the desorption process of rubidium and cesium atoms off the surface of helium nanodroplets upon excitation of the perturbed 6*s* and 7*s* states, respectively. Both experimental and theoretical results are well represented by the pseudodiatomic model for effective masses of the helium droplet in the desorption reaction of $m_{\mathrm{eff}}/m_{\mathrm{He}} \approx 10$ (Rb) and 13 (Cs). Deviations from this model are found for Rb excited to the 6*p* state. Photoelectron spectra indicate that the

[*]To whom correspondence should be addressed

[†]Physikalisches Institut, Universität Freiburg, 79104 Freiburg, Germany

[‡]Departament ECM, Facultat de Física and IN^{2}UB, Universitat de Barcelona, 08028 Barcelona, Spain

[¶]Department of Chemistry and Biochemistry, California State University at Northridge, 18111 Nordhoff St., Northridge, CA 91330, USA

[§]Laboratoire de Chimie Physique Moléculaire, Swiss Federal Institute of Technology Lausanne (EPFL), 1015 Lausanne, Switzerland

dopant-droplet interaction induces relaxation into low-lying electronic states of the desorbed atoms in the course of the ejection process.

Introduction

Helium nanodroplets are fascinating many-body quantum systems which feature unique properties such as an extremely low internal temperature (0.38 K), nanoscopic superfluidity, and the ability to efficiently cool and aggregate embedded species (dopants). Therefore, He nanodroplets are widely used as nearly ideal spectroscopic matrices for high resolution spectroscopy of isolated atoms, molecules, and clusters.[1–4]

While most studies so far pertain to the structure and time-independent spectroscopy of doped He nanodroplets, the dynamics initiated by laser-excitation or ionization of either the dopants or the droplets themselves moves into the focus of current research. A limited number of time-resolved experiments has been carried out with pure[5,6] and doped He droplets[7–14] using femtosecond pump-probe techniques. Likewise, theoretical models of pure and doped He nanodroplets have mostly been restricted to static structure and to excitation spectrum calculations.[4,15–18] Only recently, the development of time-dependent density functional theory (TDDFT) methods applicable to microscopic superfluids[19,20] has opened the way to a time-dependent description of doped He droplets in a range of sizes comparable to those used in the experiment.[21–24]

Dopants consisting of alkali (Ak) metal atoms or molecules are particularly interesting due to their weak attractive interaction with He droplets which results in their location in shallow dimple states at the droplet surface.[25–27] Upon electronic excitation, Ak atoms tend to desorb off the He droplet as a consequence of the repulsive interaction caused by the overlap of their extended electronic orbitals with the surrounding He.[28–30] The only known exceptions are Rb and Cs atoms excited to their lowest excited states.[31,32]

The dynamics of the desorption process of excited Ak atoms off the surface of He droplets has been recently studied in detail experimentally using the velocity-map imaging technique applied

to Li, Na and Rb atoms, and theoretically using TDDFT for Li and Na.[22,33] The calculated He droplet response following the dopant excitation process from ns to $(n+1)s$ states was found to be quite complex involving different types of density waves propagating through the droplet while the Ak dopant is ejected within a few picoseconds.[22] In spite of this, the experiments show that the kinetic energy of the desorbed atom depends linearly on the excitation energy of the dopant. This conspicuous result, also reproduced by the TDDFT simulations, gives further support to the pseudodiatomic model which has already been successfully applied to interpreting the absorption spectra as well as the ion velocity distributions.[33–37] According to this model, the dynamics of the excited $AkHe_N$ complex follows that of a dissociating diatomic molecule[38] where He_N plays the role of one single atom in this pseudo-diatom. The part of the He droplet that effectively interacts with the Ak atom was found to have an effective mass $m_{\text{eff}} \approx 15$ and $m_{\text{eff}} \approx 25$ amu for Li and Na, respectively.[22]

In the present work, we extend previous ion imaging and TDDFT studies to the heaviest stable Ak metal atoms Rb and Cs. We again find linear dependences of the ion kinetic energies upon laser photon energy in both experiment and theory. From these we infer the effective mass of the interacting He droplet for the desorption of Rb and Cs excited to the perturbed $6s$ and $7s$ states, respectively.

While most excited Ak atoms interact repulsively with a He nanodroplet as a whole, some excited states experience local attraction with one or a few He atoms. Therefore, as the excited Ak atom is expelled from the droplet surface, a bound AkHe molecule or in some cases small $AkHe_n$, $n = 2,3$ complexes can form.[7,29,39–42] These so called 'exciplexes' are characterized by having bound vibronic states as long as the complex is electronically excited. Upon spontaneous decay into the electronic ground state the exciplex decomposes. For such excited states of the Ak atom, the desorption dynamics may be expected to deviate from that described by the simple dissociating pseudo-diatom model.

In our previous experiment on Rb-doped He droplets excited into the $6p\Pi$ state, the ion kinetic energy distributions indicated that desorption of excited Rb atoms and RbHe exciplexes proceeds

along the repulsive pseudodiatomic potential which correlates to the closest-lying excited $6p$ state of the free Rb atom. However, the photoelectron spectra clearly revealed that a large fraction of the desorbed Rb atoms have electronically relaxed into lower-lying levels. The photoelectron spectra contained components of the $6p$ state and of lower-lying levels ($4d$ and $5p_{3/2}$).[33]

Previously, droplet-induced relaxation of excited Rb atoms was only observed within the $5p_{3/2,1/2}$ fine-structure doublet.[40] For Rb and Cs injected into bulk superfluid He fast relaxation of the lowest excited $p_{3/2}$ state into the $p_{1/2}$ and probably to the $s_{1/2}$ ground state was found to proceed within ~ 30 ps.[43]

For Na-doped He nanodroplets, droplet-induced electronic relaxation was first observed only for higher-lying excitations with principal quantum numbers $n > 6$, where the dopant-droplet interaction induces significant mixing of electronic configurations.[36] In a more recent study, even for the $3d$, $5s$ and $4d$-states the authors found indications for droplet-induced decay into lower-lying levels.[44] Interestingly, the presence of the relaxation channels was also visible in the speed distributions of the desorbed atoms, which contained multiple components. High-lying Rydberg states were found to completely relax into levels $n \leq 7$. Based on these observations, the authors suggested that droplet-induced relaxation proceeds via level-crossings of the pseudodiatomic potential curves which occur while the local He droplet environment of the excited Na dopant dynamically rearranges. Efficient He droplet-induced electronic relaxation was also observed for barium[45] and for the transition metal atoms silver,[46] chromium[47] and copper,[48] which are submerged in the droplet interior.

Note, however, that the light Ak metals Li and Na were not found to electronically relax by droplet interactions when excited into the lowest excited s-states (orbital angular momentum $\ell = 0$).[22] In contrast, in the present study on Rb and Cs atoms in their lowest excited s-states we detect *exclusively* relaxed electronic levels in the photoelectron spectra. We discuss the apparent discrepancy between the ion and electron measurements in terms of the desorption dynamics and electron energetics.

Experimental

The experiments presented here are performed using the same setup as described previously.[33] In short, a continuous beam of He nanodroplets with a mean size ranging from 200 to 17000 He atoms per droplet is generated by varying the temperature T_0 of a cryogenic nozzle with a diameter of 5 μm.[2,3] An adjacent vacuum chamber contains a vapor cell filled with bulk metallic Rb or Cs heated to 85°C and 70°C, respectively. In the detector chamber further downstream, the He droplet beam intersects a dye laser beam (Sirah Cobra, pulse length 10 ns, pulse energy 10 μJ, repetition rate 1 kHz) at right angles in the center of a velocity map imaging (VMI) spectrometer. The laser is linearly polarized along the direction of the He droplet beam, which is perpendicular to the symmetry axis of the VMI spectrometer. We record single events per image frame for which the coordinates are determined using the centroid method. Velocity-map photoelectron and photoion images are transformed into kinetic energy distributions using standard Abel inversion programs.[49,50]

Theoretical approach

In order to model the absorption spectra as well as the dynamic response of the excited doped He droplets we describe the doped He droplets within the Density Functional Theory (DFT) framework.[4] The basic ingredients of our approach are described in detail in Refs.[22,23] Let us just recall that we have used the Born-Oppenheimer approximation to factorize the electronic and nuclear wavefunctions, the Franck-Condon approximation which assumes that the atomic nuclei do not change their positions or momenta during the electronic transition, and the diatomics-in-molecules approximation (pseudodiatomic model).[51]

We have first obtained the structure of the Rb-droplet and Cs-droplet complexes in the ground state. Throughout this work we have used the Orsay-Trento (OT) density functional[52] neglecting the backflow term. The Rb-He and Cs-He ground state pair potentials V_X have been taken from Ref.[53] Due to the large mass of Rb and Cs compared to that of He, we describe them as classical

particles in the dynamics while their effect in the statics is incorporated as an external field acting upon the droplet.[23] Accordingly, the energy of the system is written as

$$\begin{aligned} E[\rho] &= \int d\mathbf{r}\, \frac{\hbar^2}{2m_{\mathrm{He}}} \left|\nabla\sqrt{\rho(\mathbf{r})}\right|^2 + \mathscr{E}_{\mathrm{He}}[\rho(\mathbf{r})] \\ &+ \int d\mathbf{r}\rho(\mathbf{r}) V_X(|\mathbf{r}_{\mathrm{Ak}} - \mathbf{r}|)\,, \end{aligned} \tag{1}$$

where $\mathscr{E}_{\mathrm{He}}$ is the OT potential energy density per unit volume, Ak represents either the Rb or Cs atom, and ρ is the He particle density. Upon variation, one obtains the Euler-Lagrange equation that has to be solved to determine the equilibrium density $\rho_0(\mathbf{r})$ of the droplet and the location of the dopant Rb or Cs atom $\mathbf{r}_{\mathrm{Ak}_0}$.[35] Schematically,

$$\frac{\delta}{\delta\rho}\left(\frac{\hbar^2}{2m_{\mathrm{He}}}\left|\nabla\sqrt{\rho}\right|^2 + \mathscr{E}_{\mathrm{He}}\right) + V_X = \mu\,, \tag{2}$$

where μ is the chemical potential of the He droplet that throughout this paper is made of $N = 1000$ atoms. To explore other locations of the Ak atom around its equilibrium position in the surface dimple, we have minimized the energy submitted to a constraint.[23] This will be useful for determining the mean kinetic energy of the ejected Ak atom as a function of the excess excitation energy.

Equation (**??**) has been solved in cartesian coordinates using a spatial grid of 0.4 Å and a $200 \times 200 \times 250$ points mesh. The derivatives have been calculated with 13-point formulas. Extensive use of fast-Fourier techniques has been made to efficiently calculate the energy density and dopant-droplet interaction potentials.[22,23]

The dynamics is triggered by the sudden substitution of the Ak-He ground state pair potential by the excited one. Within TDDFT, we represent the He droplet by a complex effective wavefunction $\Psi_{\mathrm{He}}(\mathbf{r},t)$ such that $\rho(\mathbf{r},t) = |\Psi_{\mathrm{He}}(\mathbf{r},t)|^2$. The position of the Ak atom $\mathbf{r}_{\mathrm{Ak}}(t)$ obeys Newton's equation. For excitations involving two *s* states, the evolution equations derived in Ref.[23] adopt a

simple form, namely

$$
\begin{aligned}
i\hbar\frac{\partial}{\partial t}\Psi_{\mathrm{He}} &= \left[-\frac{\hbar^2}{2m_{\mathrm{He}}}\nabla^2+\frac{\delta\mathscr{E}_{\mathrm{He}}}{\delta\rho(\mathbf{r})}+V_{ns}(\mathbf{r}-\mathbf{r}_{\mathrm{Ak}})\right]\Psi_{\mathrm{He}} \\
m_{\mathrm{Ak}}\ddot{\mathbf{r}}_{\mathrm{Ak}} &= -\nabla_{\mathbf{r}_{\mathrm{Ak}}}\left[\int d\mathbf{r}\rho(\mathbf{r})V_{ns}(\mathbf{r}-\mathbf{r}_{\mathrm{Ak}})\right] . \qquad (3)
\end{aligned}
$$

In the above equations, V_{ns} with $n = 6(7)$ is the $6s(7s)$ excited Rb(Cs)-He pair potential.[54] The initial configuration to solve Eqs. (3) is the static dopant-droplet configuration, either at equilibrium or with the dopant sitting in another position around the surface dimple, $\Psi(\mathbf{r},t=0)=\sqrt{\rho_0(\mathbf{r})}$, $\mathbf{r}_{\mathrm{Ak}}(t=0)=\mathbf{r}_{\mathrm{Ak}_0}$. The initial velocity of the Ak dopant is set to zero.

Equations (3) have been solved using the same grid as for the static problem and a time step of 0.5 fs. We have used a predictor-corrector method[55] fed by a few time steps obtained by a fourth-order Runge-Kutta algorithm.

Photoions

In this work we focus on the $ns\Sigma \rightarrow (n+1)s\Sigma$ transitions of the $RbHe_N$ and $CsHe_N$ pseudo-diatoms, where $n = 5, 6$ denotes the principal quantum number of the atomic ground states of Rb and Cs, respectively. The excitation scheme is represented in Fig. 1 for Rb, where we use the pseudodiatomic potential energy curves computed by Callegari and Ancilotto.[30] The ionic potential is obtained by integration of the Rb^+-He pair potential[56] over the He density distribution corresponding to the Rb ground state configuration, which we assume to be frozen.[35] Since the Ak-He interaction in the excited $(n+1)s\Sigma$ states is purely repulsive, the excited Ak atoms detach from the He droplets as neat atoms. Subsequent ionization by the absorption of a second photon from the same nanosecond laser pulse yields atomic ions which we detect with the VMI spectrometer.

Using these potentials,[30] we have obtained the Rb and Cs absorption spectra by calculating wave functions and Franck-Condon factors for the pseudodiatomic transitions using R. LeRoy's program BCONT 2.2 .[57] The results are depicted in Fig. 2. We have also calculated the Rb $5s\Sigma \rightarrow$

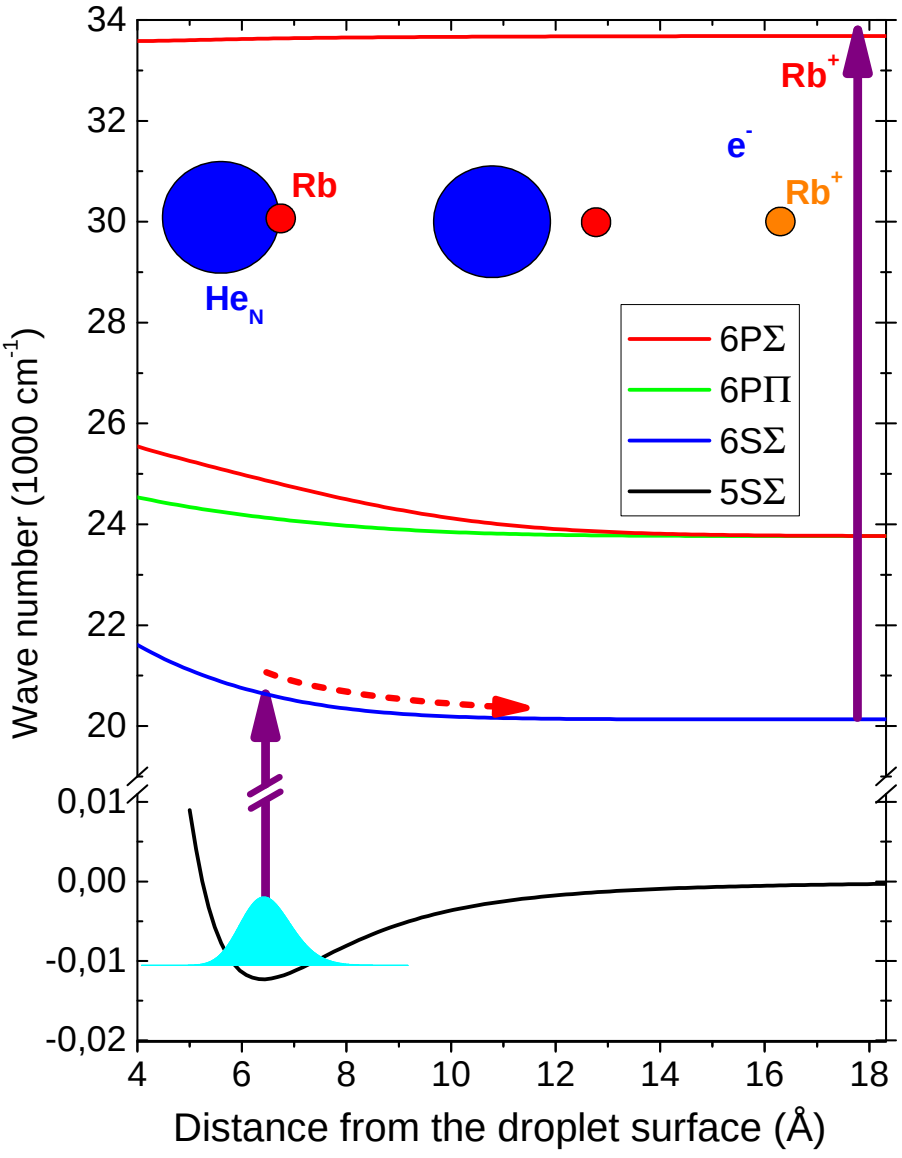

Figure 1: Sketch of the excitation and ionization scheme of Rb attached to He nanodroplets. Upon excitation of the $RbHe_N$ complex to a repulsive pseudodiatomic potential,[30] the Rb atom departs from the droplet surface and is ionized by a second photon from the same laser pulse.

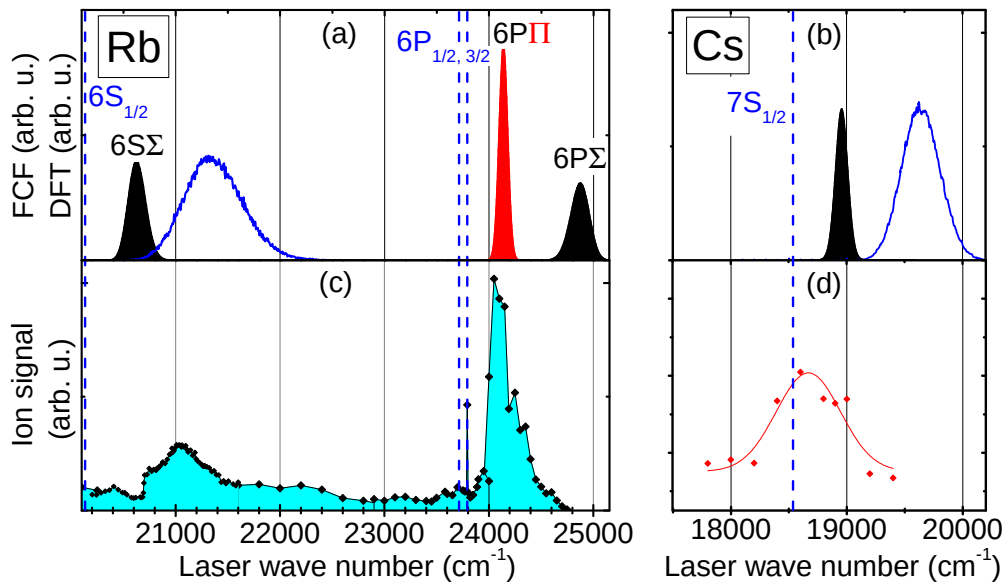

Figure 2: Simulated (a, b) and measured (c, d) photoionization spectra of He nanodroplets doped with Rb and Cs. The filled curves in (a, b) show Franck-Condon calculations based on Rb-He$_N$ and Cs-He$_N$ pseudodiatomic potentials;[30] the blue lines show the Rb $6s\Sigma$ (a) and Cs $7s\Sigma$ (b) absorption profiles obtained from the present atomic-like DFT sampling method.

$6s\Sigma$ and Cs $6s\Sigma \rightarrow 7s\Sigma$ absorption band contours by employing the atomic-like DFT sampling method described in Ref.,[21,58] shown in that figure as blue lines. The vertical dashed lines indicate the atomic transitions.

Both experimental and theoretical absorption spectra are characterized by broad bands which are blue-shifted with respect to the free atomic transitions. The blue-shift of the transitions of Rb attached to He droplets results from the fact that all excited pseudodiatomic potentials are repulsive whereas the ground state is slightly attractive (Fig. 1). The widths of the absorption contours reflect the width of the ground state wave function which is mapped onto the excited repulsive potential upon excitation. While the calculated Franck-Condon profile of the Rb $6p\Pi$ transition and the experimental spectrum is satisfactory, the Franck-Condon profile of the $6s\Sigma$ transition is slightly red-shifted with respect to the experimental contour, whereas the DFT result is blue-shifted (Fig. 2 a and c). The photoionization spectrum of Cs (Fig. 2 d) features a maximum in the range $\sim$ 18300-19000 cm^{-1} associated with the $7s\Sigma$ transition. The corresponding DFT calculation (Fig. 2 b) yields a peak centered at 19635 cm^{-1}, which is again significantly blue-shifted. The

DFT calculation thus overestimates the atomic shift, being unclear which part of the disagreement has to be attributed to deficiencies of the model and which to inaccuracies of the excited Ak-He pair potentials we are using.[54]

Note that a broad Rb^+ ion signal level which features a step around 20 700 cm^{-1} is measured around the $6s\Sigma$ feature, as previously observed in photoion[33] and laser-induced fluorescence spectra[59] around the $6p\Pi$ transition. This contribution may be due to photoionization of Rb_2 dimers which fragment into Rb^+. In particular, at wave numbers below 20 700 and above 21 000 cm^{-1} we observe significant Rb_2^+ signals in the tof mass spectrum which could be due to resonance-enhanced ionization via the $2^3\Sigma_u$ and via the $2^1\Sigma_u$, $2^1\Pi_u$, or $3^3\Pi_g$ states of Rb_2, respectively.[60]

The dynamics of the laser-induced desorption process of Rb and Cs atoms is studied by recording velocity-map ion images. Fig. 3 (a) and (b) displays the raw and inverted Rb^+ ion images taken upon excitation to the $6s\Sigma$ state of the $RbHe_N$ complex at the laser wave number $\bar{\nu} = 20\,800\,cm^{-1}$. The image features a circular intensity distribution with a pronounced anisotropy of the angular dependence. The intensity maxima are directed along the polarization axis of the laser (yellow arrow), as expected for the parallel $5s\Sigma \rightarrow 6s\Sigma$ transition.[22,33] The velocity-map ion images of Cs recorded at the $6s\Sigma \rightarrow 7s\Sigma$ transition around $\bar{\nu} = 18\,700$ cm^{-1} closely resemble those for Rb. In the measurements of Rb excited to the $5p\Pi$ state around $\bar{\nu} = 24\,100$ cm^{-1}, the opposite anisotropy is observed as expected for a perpendicular $\Sigma \rightarrow \Pi$ transition in the frame of the pseudodiatomic model.[33]

From these images we infer the ion kinetic energy distributions (KED) by applying inverse Abel transformation and angular integration. Typical examples of such KED for excitation around the maximum of the $6s\Sigma$ band are depicted in Fig. 3. Similarly to the previous measurements with Li and Na,[22] the KED consist of well-resolved maxima of widths ~ 70 meV which shift toward higher kinetic energies as the photon energy increases.

Figure 4 presents a compilation of the results of the analysis of the ion images recorded around the Rb $6s\Sigma$ band as a function of the laser wave number. The total Rb^+ ion counts [black squares in a)] reproduce the photoionization spectrum (red diamonds) with some systematic deviation at

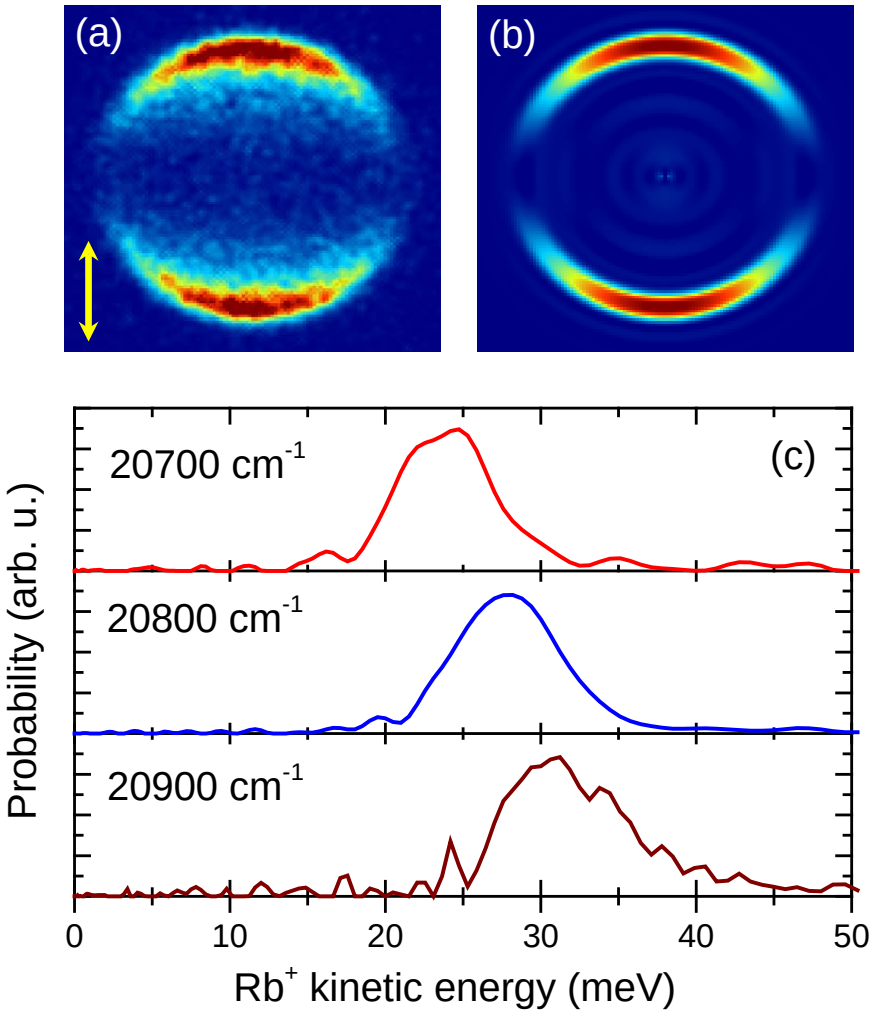

Figure 3: Top: Raw (a) and inverse Abel transformed (b) velocity-map Rb^+ ion images recorded when exciting Rb atoms attached to He nanodroplets on the transition $5s\Sigma \rightarrow 6s\Sigma$ at the laser wave number $\bar{\nu} = 20\,800\,\mathrm{cm}^{-1}$. The laser polarization direction is indicated by the vertical arrow. Bottom: Rb^+ ion kinetic energy distributions inferred from ion images recorded at the indicated laser wave numbers.

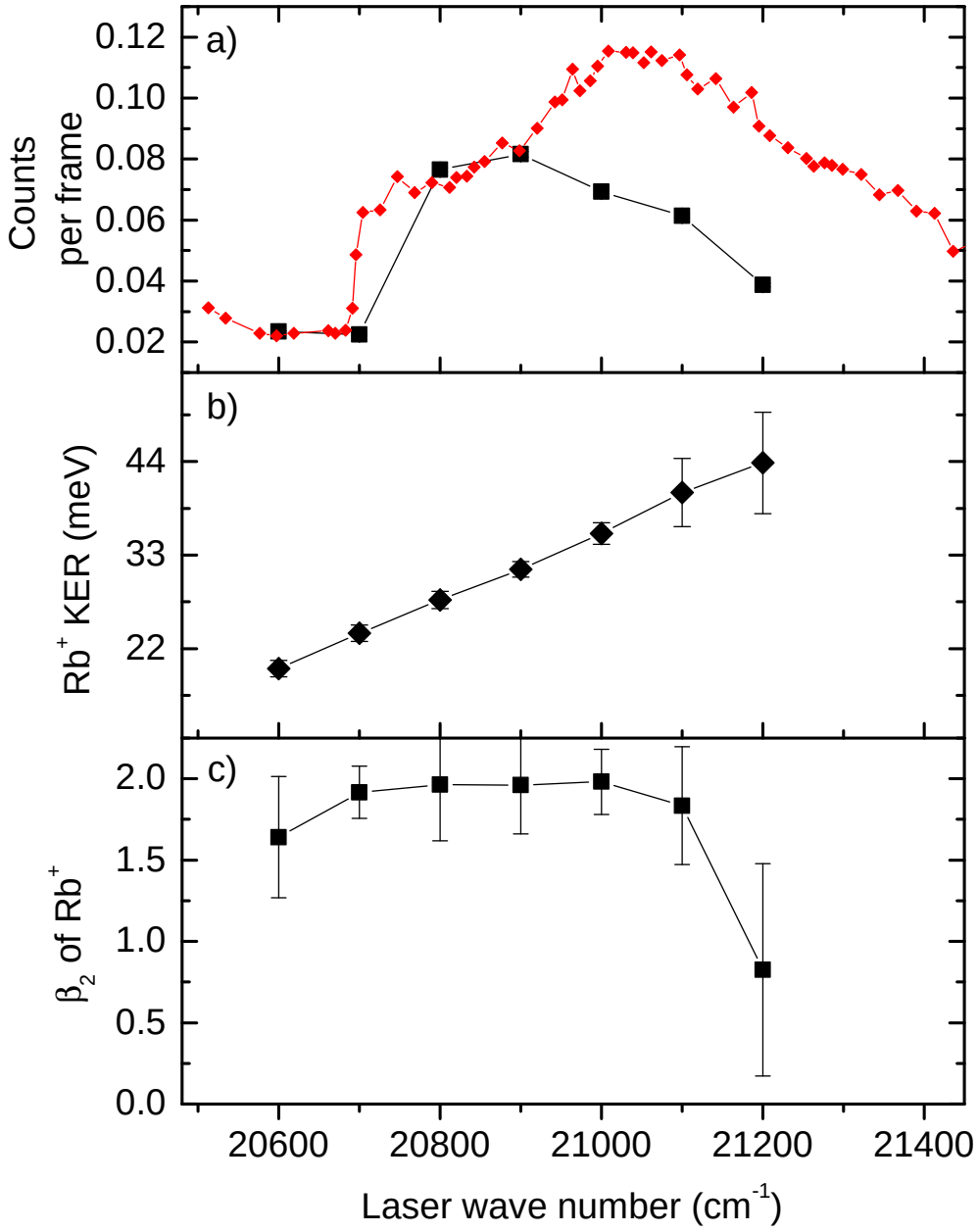

Figure 4: (a) Total Rb^+ ion counts and tof peak intensity (red), (b) Rb^+ mean kinetic energies, (c) anisotropy parameters β_2 inferred from ion images recorded at various laser wavelengths around the maximum of the Rb $6s\Sigma$ absorption band.

wave numbers $>20\,850$ cm^{-1} of unknown origin. The mean values of the KED inferred from the images, shown in Fig. 4 (b), nearly linearly increases with laser wave number. In addition, Fig. 4 (c) shows the variation of the anisotropy parameter β_2 within a 4 sigma range around the KED intensity maximum inferred from the angular distributions $I(\theta)$ by fitting to the general expression for the probability distribution of one-photon transitions $I(\theta) \propto 1 + \beta_2 P_2(\cos\theta)$.[61] For laser wave numbers close to the maximum of the $6s\Sigma$ absorption band (20700-21100 cm^{-1}) we obtain beta=1.9(3). Within the experimental error this is consistent with the value $\beta_2 = 2$ expected for excitation of an ideal diatomic molecule at a parallel $\Sigma - \Sigma$ transition. In this case the angular distribution of dissociation products takes the form $I(\theta) \propto \cos^2\theta$.

This result nicely confirms the validity of the pseudodiatomic model and the assignment of the spectral band to the parallel $5s\Sigma \rightarrow 6s\Sigma$ transition. However, in the wings of the absorption peak we find the anisotropy of the angular ion distribution to be significantly reduced. This may be due to the contribution of fragment ions from Rb_2 dimers which are present to a small extent in the droplet beam. Besides, it is conceivable that dynamic deformations of the local He droplet environment during the departure of the Rb atom induce perturbations of the electronic configuration of the excited Rb atom which are not accounted for in the pseudodiatomic picture.

In order to obtain more detailed insight into this process, we have simulated the ejection of a Rb atom from the nominal $6s$ state and of a Cs atom from the nominal $7s$ state using TDDFT calculations. The velocities and positions as a function of time for Rb and Cs ejected from the equilibrium position at the surface dimple are shown in Fig. 5. It can be seen that the Cs atom reaches an asymptotic velocity of ~ 230 m/s after a time evolution of ~ 1.25 ps. By this time, the Cs atom is ~ 2 Å away from its original equilibrium position at the dimple. The corresponding values for the Rb atom are ~ 350 m/s, ~ 1 ps and ~ 2.7 Å, respectively. In both cases, the recoil velocity of the He droplet is small, of the order of 7.5 m/s. The different evolution of positions and velocities for Rb and Cs is mainly due to the different masses of the two species. The fact that both curves are smooth and monotonously increasing with time implies that the desorption proceeds impulsively. Thus, although in the first stages of the dynamics surface vibrations and highly non-

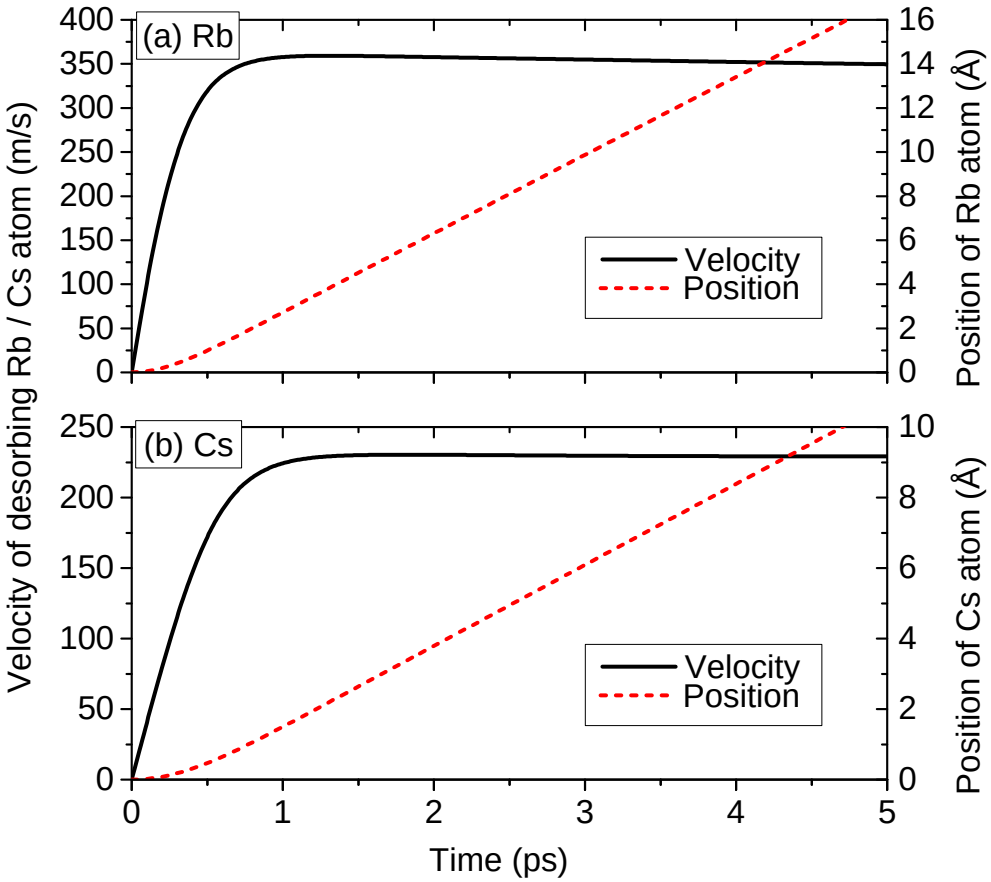

Figure 5: (Color online) Velocity (solid line, left scale) and displacement from its equilibrium location at the surface dimple (dashed line, right scale) of the desorbing Rb (a) and Cs (b) atoms as a function of time after excitation of the $6s\Sigma$ state.

linear density waves are excited in the droplet which take a large part of the energy deposited in the system upon photo excitation, the desorption dynamics is rather insensitive to them.

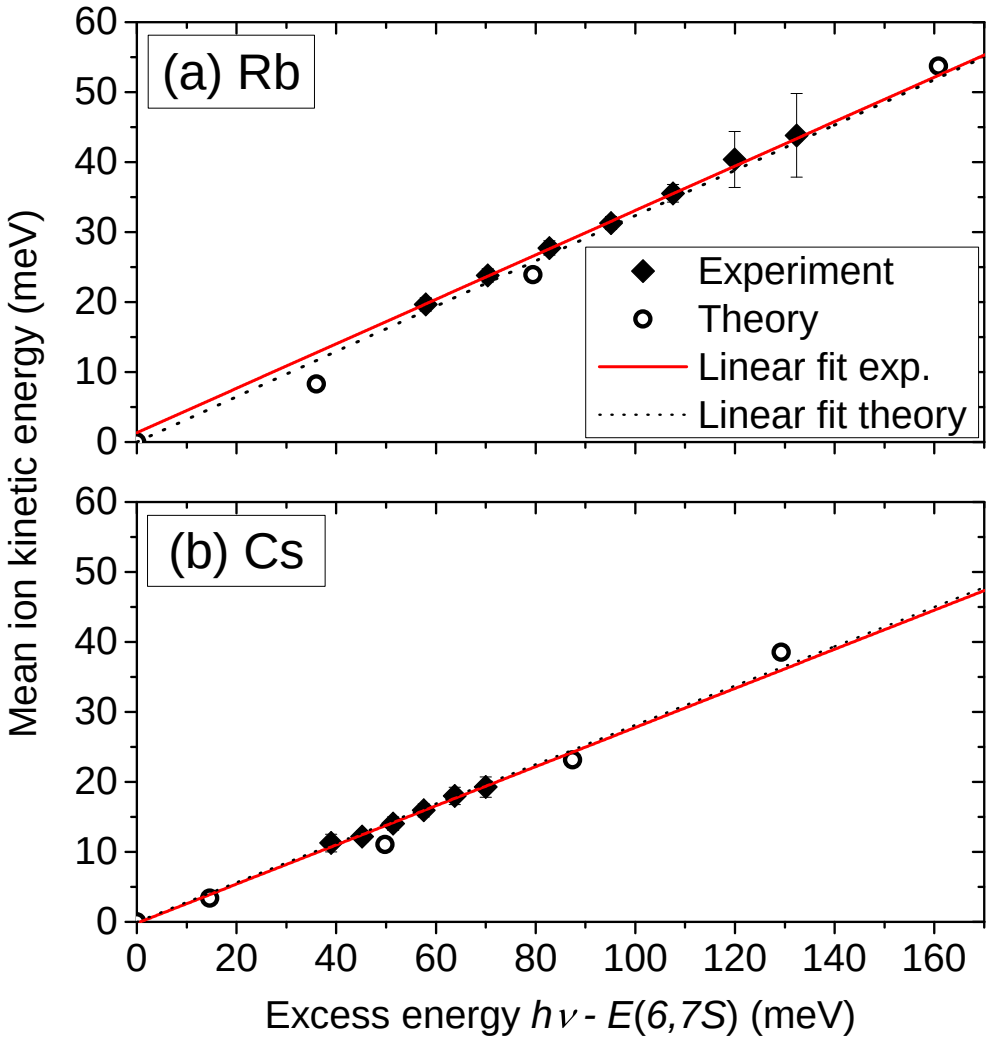

Figure 6: Mean kinetic energies of desorbed Rb (a) and Cs (b) atoms upon excitation to the 6*s*Σ and 7*s*Σ states, respectively. Straight lines: linear fits to the theoretical and experimental data.

Detailed information about the kinematics of the desorption process can be gained from the kinetic energies of the desorbing dopants as a function of the excess excitation energy (difference between photon energy and internal energy of the free Rb or Cs atom in the 5*s* and 6*s* states).[22] The results are shown in Fig. 6 and compared to the experimental mean kinetic energies. The calculated points have been obtained by starting the dynamic simulation from different positions of the Ak obtained by a constrained minimization of the total energy of the Ak-He_N complex as

indicated in Sec. III.

For both Rb and Cs dopants, the kinetic energy displays a linear dependence on the excess excitation energy. This dependence indicates that in spite of its apparent complexity, the ejection process is well represented by the pseudodiatomic model.[22,38] Indeed, imposing the energy and linear momentum conservation in the instantaneous ejection of the Ak atom from the droplet one obtains

$$E_{kin} = \eta(\hbar\omega - \hbar\omega_0) \, . \tag{4}$$

Here, ω denotes the laser frequency and ω_0 is the atomic transition frequency. Within this model, the value of the slope η is related to the mass m_{eff} of the part of the He droplet that effectively interacts with the Ak atom[22] by

$$\eta = \frac{m_{\text{eff}}}{m_{\text{eff}} + m_{\text{Ak}}} \Longrightarrow m_{\text{eff}} = \frac{\eta}{1-\eta} m_{\text{Ak}} \, . \tag{5}$$

By fitting the experimental and simulation data to the expression Eq. (**??**) one obtains a theoretical value $m_{\text{eff}} \sim 40.7$ amu (10.2 He atoms) for Rb as compared with the experimental value of 39.6 amu (9.9 He atoms). The corresponding values for Cs are $m_{\text{eff}} \sim 52.0$ amu (13.0 He atoms) from theory and 51.6 amu (12.9 He atoms) from experiment. The results for Rb and Cs, together with those obtained for Li and Na in Ref.,[22] are collected in Table 1 and plotted in Fig. 7. One observes an increase of m_{eff} with the mass of the Ak atom, as indicated by Eq. (**??**), although the prefactor $\eta/(1-\eta)$ has the opposite behavior.

The conspicuous dependence of the effective mass of the helium droplet m_{eff} on the Ak dopant mass m_{Ak} is expected to be mainly determined by two effects. On the one hand, the geometric structure of the excited Ak-droplet system is different for each species due to slight variations of the ground state equilibrium configuration[62] (radius of the surface dimple, distance of the Ak atom from the surface) as well as due to a varying mean radius of the excited Ak atom orbital r_e. On the other hand, the kinematics of the dissociation process induces an Ak mass-dependence, irrespective of the differing geometric initial conditions.

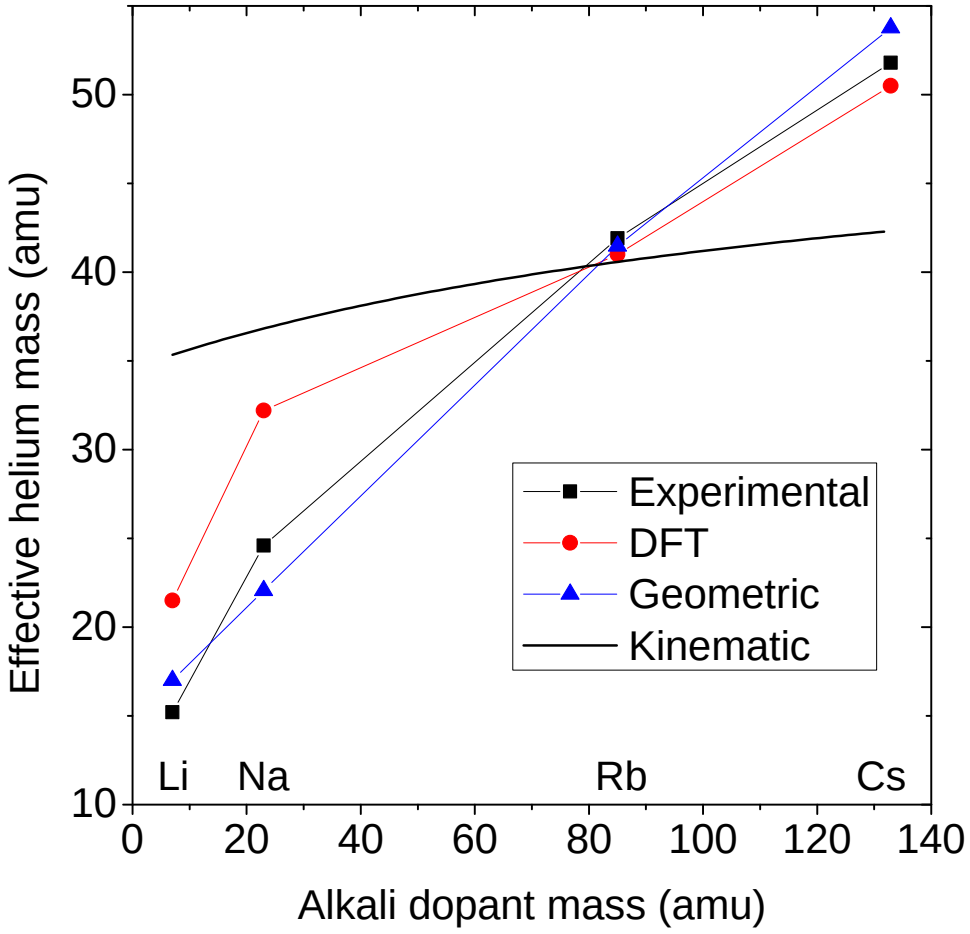

Figure 7: Experimental, theoretical and estimated values of the effective mass of the He droplet in the desorption process of various alkali species excited to their first excited *s*-states.

The geometric effect is estimated by computing the geometrical overlap of the electron orbit of the excited Ak atom with the adjacent He atoms of the dimple. Based on the He dimple parameters specified in Ref.[62] and on values for the mean orbital radius $\langle r_e \rangle$ we calculate the number of He atoms in the overlap volume V_{eff} of the excited Ak orbit and He dimple surface, $N_{\text{He,eff}} = V_{\text{eff}} \rho_{\text{eff}}$. Here, ρ_{eff} is taken as half the bulk value $\rho_{\text{He}} = 0.0218$ Å^{-3} which roughly matches the average He density within the overlap volume due to its location dimple surface where the density smoothly falls off.[62] The mean orbital radius is approximated by[44,63]

$$\langle r_e \rangle = \frac{3}{2} a_0 (n - \delta_l)^2, \tag{6}$$

where a_0 is the Bohr radius and δ_l is the quantum defect of the Ak excited state. The corresponding values of $\langle r_e \rangle$ and $N_{\text{He,eff}}$ are added to Table 1 and to Fig. 7.

The kinematic effect of the varying mass of the desorbing Ak atom is probed by solving the classical equations of motion of the Ak atom being repelled off a linear chain of effective, mutually non-interacting He atoms, each containing the mass of 7 He atoms which roughly equals the number of He atoms in the first surface layer next to the Ak dopant.[62] The initial spacing between the He "layersÂt' Ât' is taken as the average distance between He atoms in the droplets, 3.6 Å.[64] The distance between the Ak atom and the fist He "layerÂt' Ât' is held fixed at 5.5 Å and the same Ak-He interaction potential $V_{\text{Ak-He}}(d) = 0.2 \exp(-d/3 - 1)$ (in atomic units) is used for all Ak species. The trajectories of the Ak atoms closely follow those shown in Fig. 5 and the trajectories of the He layers show that mostly the first He layer participates in the desorption dynamics. Accordingly, the effective mass of the He droplet (approximated by the linear chain of atoms with the mass of the He layers) only slightly exceeds the mass of the first He layer, 28 amu, see the solid line in Fig. 7.

While the He effective mass in this simple kinematic model matches the experimental and DFT values for Rb, the variation as a function of Ak dopant mass is not sufficiently well reproduced (Fig. 7). The simple estimate based on the geometric Ak-He orbital overlap, however, shows a

strong variation of the effective mass in surprisingly good agreement with the experimental values. We therefore conclude that the difference in the number of interacting He atoms for the different Ak species is likely related to the difference in the dimple structure and excited electron orbit rather than to the kinematics of the desorption process.

The detailed picture of the dynamics of the He droplet upon excitation of the Ak atom is obtained from the DFT calculations. Fig. 8 shows the evolution of the $CsHe_{1000}$ and $RbHe_{1000}$ complexes after the Ak atom has been excited. It can be seen the dramatic changes in the droplet density caused by the excitation and subsequent ejection of the dopant.

Figure 9 shows the evolution of the He cross-sectional density profiles of a He_{1000} droplet doped with a Rb and a Cs atom for the first 5 ps. Initially, the droplet extends along the z symmetry axis from about 0 to 44 Å, and the Ak atom is located in a dimple at the droplet surface (near $z = 0$). Excitation of the Ak atom to the $(n+1)s$ state causes the dimple first to deepen due to the highly repulsive Ak-He interaction in the $(n+1)s\Sigma$ state. The associated compression of the He droplet lasts up to $\sim$ 1 ps, as shown in the figure. Following this compression, the He surface bounces back and the dimple starts being filled. The more distant part of the droplet (near $z = 42$ Å) is unperturbed and at rest, indicating that during these first ps the energy deposited in the droplet goes to its internal excitation and not to its center-of-mass motion.

Figures 8 and 9 reveal that the excitation of the Cs and Rb atoms launches highly non-linear density waves into the droplet. In the case of Rb, the first perturbation front, labeled as 1, moves at $\sim$ 900 m/s. This perturbation generates carrier waves with a phase velocity of $\sim$ 430 m/s, modulated by supersonic envelope fronts with growing intensity. The ones with highest intensity, labeled as 2, have a group velocity of $\sim$ 700 m/s. Next, a high intensity wave appears traveling at $\sim$ 410 m/s (labeled as 3), which generates secondary waves propagating backwards. In the case of Cs, the velocities of the fronts are 880 m/s, 675 m/s, and 410 m/s, respectively. A similar behavior was found in Ref.[22] for Na and Li atoms.

As an extension of our previous ion imaging measurements at the Rb $6p\Pi$ band[33] we analyze here the mean ion kinetic energy as a function of the excess energy. Since in the $6p\Pi$ configuration

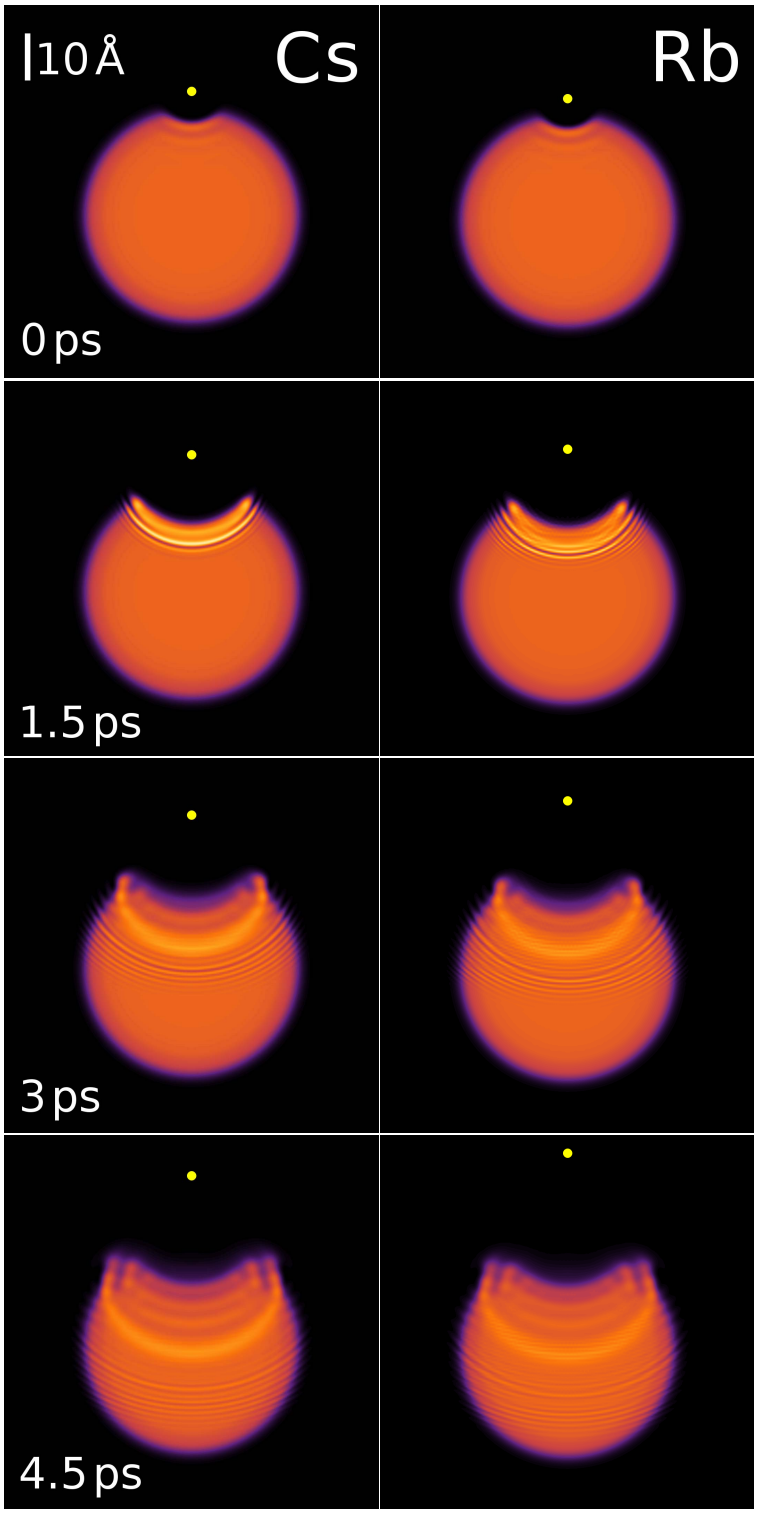

Figure 8: Evolution of the He density distributions of the $CsHe_{1000}$ (left column) and $RbHe_{1000}$ (right column) systems after excitation to their $(n+1)s\Sigma$ states. (Multimedia view)

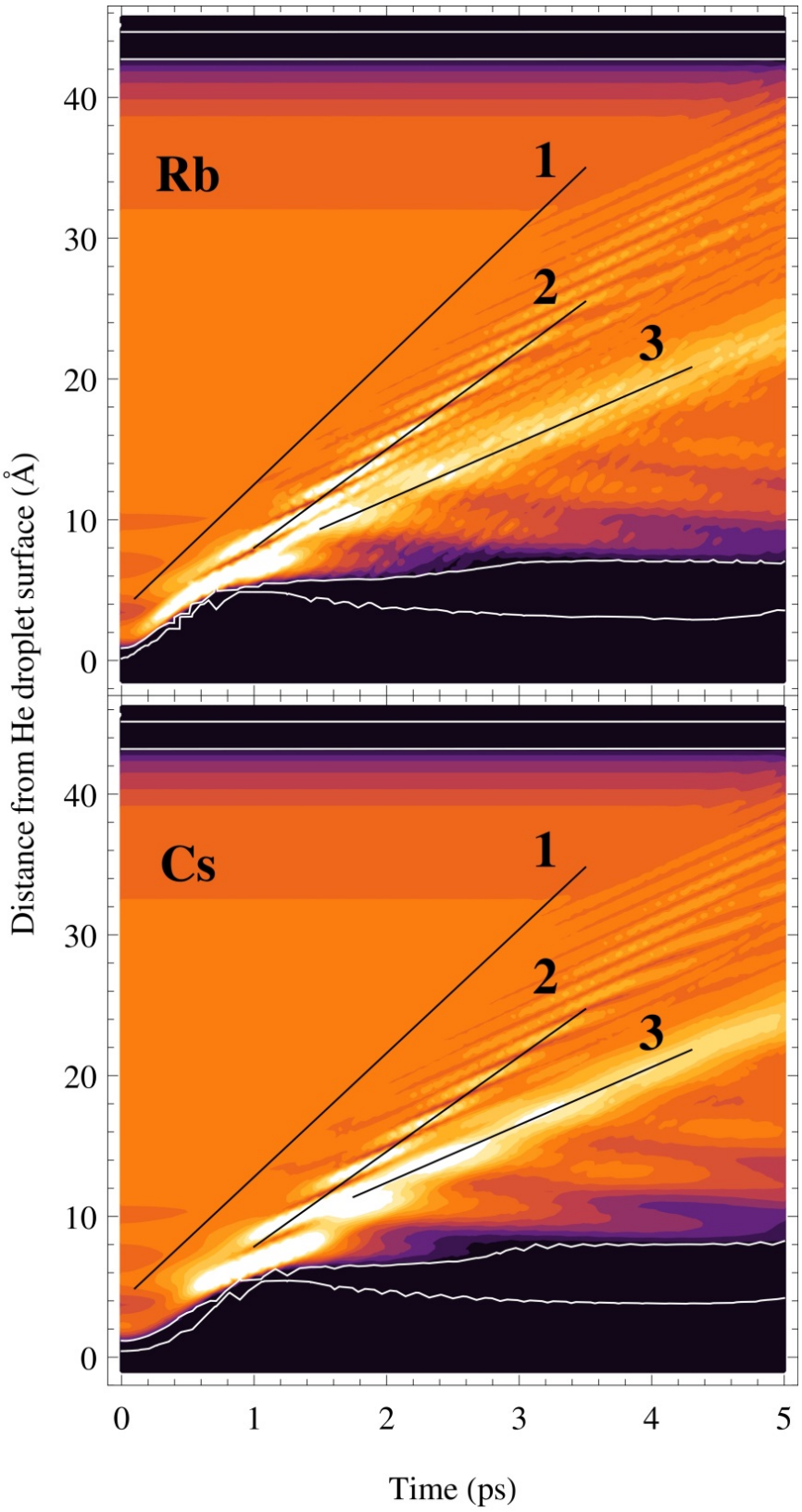

Figure 9: Evolution of the He density profile of the $AkHe_{1000}$ system along the symmetry axis. Three supersonic wave fronts are identified and labeled by 1 to 3. Equidensity lines corresponding to 0.5 and 0.1 times the He saturation density, 0.0218 $Å^{-3}$, representing the surface region of the droplet, are shown in white.

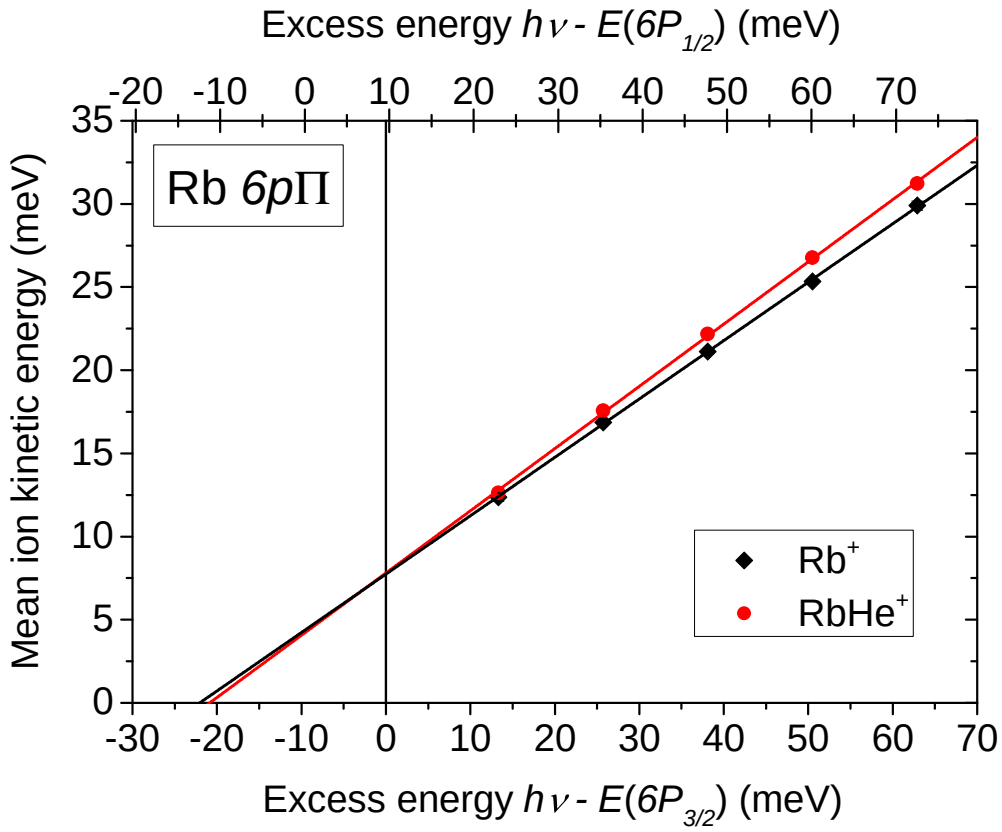
Excess energy $h\nu$ - $E(6P_{1/2})$ (meV)
-20 -10 0 10 20 30 40 50 60 70
Rb $6p\Pi$
Mean ion kinetic energy (meV)
0 5 10 15 20 25 30 35
Rb^+
$RbHe^+$
-30 -20 -10 0 10 20 30 40 50 60 70
Excess energy $h\nu$ - $E(6P_{3/2})$ (meV)

Figure 10: Experimental mean kinetic energies of Rb atoms and of RbHe exciplexes ejected out of He droplets upon excitation of the $6p\Pi$ state of the $RbHe_N$ complex. The lines are linear fits to the data.

the Rb-He pair potential along the internuclear axis is attractive,[54] RbHe exciplexes are formed with roughly 40% relative abundance.[33] Therefore, we record ion images for Rb^+ and $RbHe^+$ ions separately and extract the mean ion kinetic energies for each of the two species.

Figure 10 shows that the data points lie on a straight line that surprisingly intercepts the abscissa at a finite value of the excess energy of about -22 meV. Using Eq. (**??**), from the slope of the line η one obtains $m_{\mathrm{eff}} = 46.0$ (11.5 He atoms) for Rb, and $m_{\mathrm{eff}} = 53.2$ amu (13.3 He atoms) for RbHe, slightly larger than the corresponding value for the $6s\Sigma$ state.

The fact that the extrapolation of the $6p\Pi$ experimental data to zero kinetic energy yields a finite energy shift at zero kinetic energy, at variance with the extrapolation of the $6s\Sigma$ data, discloses an intrinsic limitation of the method used to analyze the results. The pseudodiatomic approximation, even if appropriate for the description of a direct dissociation via a purely repulsive state, does not account for other effects which are present in the dissociation kinematics of the $(n+1)p$ excitation. In the case of the $6p\Pi$ state of Rb, the dopant-He interaction contains both repulsive and attractive contributions, the latter inducing the formation of exciplexes. It is conceivable that the binding energy of the RbHe exciplex may be converted into additional translational energy upon desorption of RbHe. This interpretation has recently been invoked to rationalize the negative excess energy offset measured for NaHe exciplexes formed upon excitation of Na into the droplet-perturbed $3d$ state.[44] The binding energy of RbHe in the $6p\Pi$ state amounts to about 8 meV, which does not account for the observed energy shift alone. Additional internal energy may be released into translational motion of the desorbing Rb by droplet-induced relaxation of population from the upper $6p_{3/2}$ into the lower $6p_{1/2}$ spin-orbit state of Rb. In that case, the excess energy axis would be down-shifted as represented by the horizontal top scale of Fig. 10 provided the droplet effective mass is the same ($m_{\mathrm{eff}} = 46.0$ amu) for this additional acceleration of the Rb atom due to spin-orbit relaxation. However, the atomic spin-orbit splitting (9.6 meV) does not fully account for the observed shift. Only the assumption that both spin-orbit and binding energy of the RbHe exciplex are fully converted into translational energy would explain the energy offset for RbHe. The nearly coinciding kinetic energies of Rb and RbHe may indicate that Rb^+ ions are actually produced by

dissociative ionization of RbHe, the latter being the dominant product of the desorption reaction.

Thus, it seems that the pseudodiatomic model no longer strictly applies when the internal degrees of freedom of the constituent atom are involved in the dynamics. Note that for the case of the desorption of sodium (Na) atoms excited to the $3p$ state deviations from the pseudodiatomic model were also observed.[65] However, in contrast to the Rb case discussed here, a positive value for the abscissa intercept was found. TDDFT studies of Ak atoms ejected from the $(n+1)p$ excited states could help elucidate this open issue, but improved Ak-He pair potentials have to be previously obtained.

Photoelectrons

Complementary information about the dynamics following laser excitation of Ak atoms attached to He nanodroplets is obtained from imaging photoelectrons. In the experiment, velocity-map photoelectron images are obtained by simply reversing the polarity of the voltages applied to the repeller and extractor electrodes.[33] A typical raw and inverse Abel transformed image recorded at the laser wave number $\bar{\nu} = 21\,400$ cm^{-1} is depicted in the upper and lower half of Fig. 11 (a), respectively. The image clearly contains three separated ring structures, indicating that ionization occurs out of three Rb atomic orbitals. The faint ring structure between the two inner rings in the low half of Fig. 11 (a) is an artifact of the inverse Abel tranformation caused by the limited statistics. As for the ion images, we again convert the electron images into angular distributions and electron kinetic energy spectra. The latter are shown in Fig. 11 (b) for Rb and in (c) for Cs.

Surprisingly, all the photoelectron spectra recorded within the Rb $6s\Sigma$ band reveal contributions of the Rb $5p_{1/2}$, $5p_{3/2}$ and $4d$ atomic levels. No electron signal associated with the $6s$ state is detected within the noise level, although the $6s$ state is the dominant atomic component of the originally excited $6s\Sigma$ state of the RbHe$_N$ complex.[30] The same holds for Cs excited to the $7s\Sigma$ state. Only one peak is present in the spectrum due to ionization out of the Cs $5d$ state. The $6p$ states, which are probably populated as in the Rb case, are not detected because of insufficient

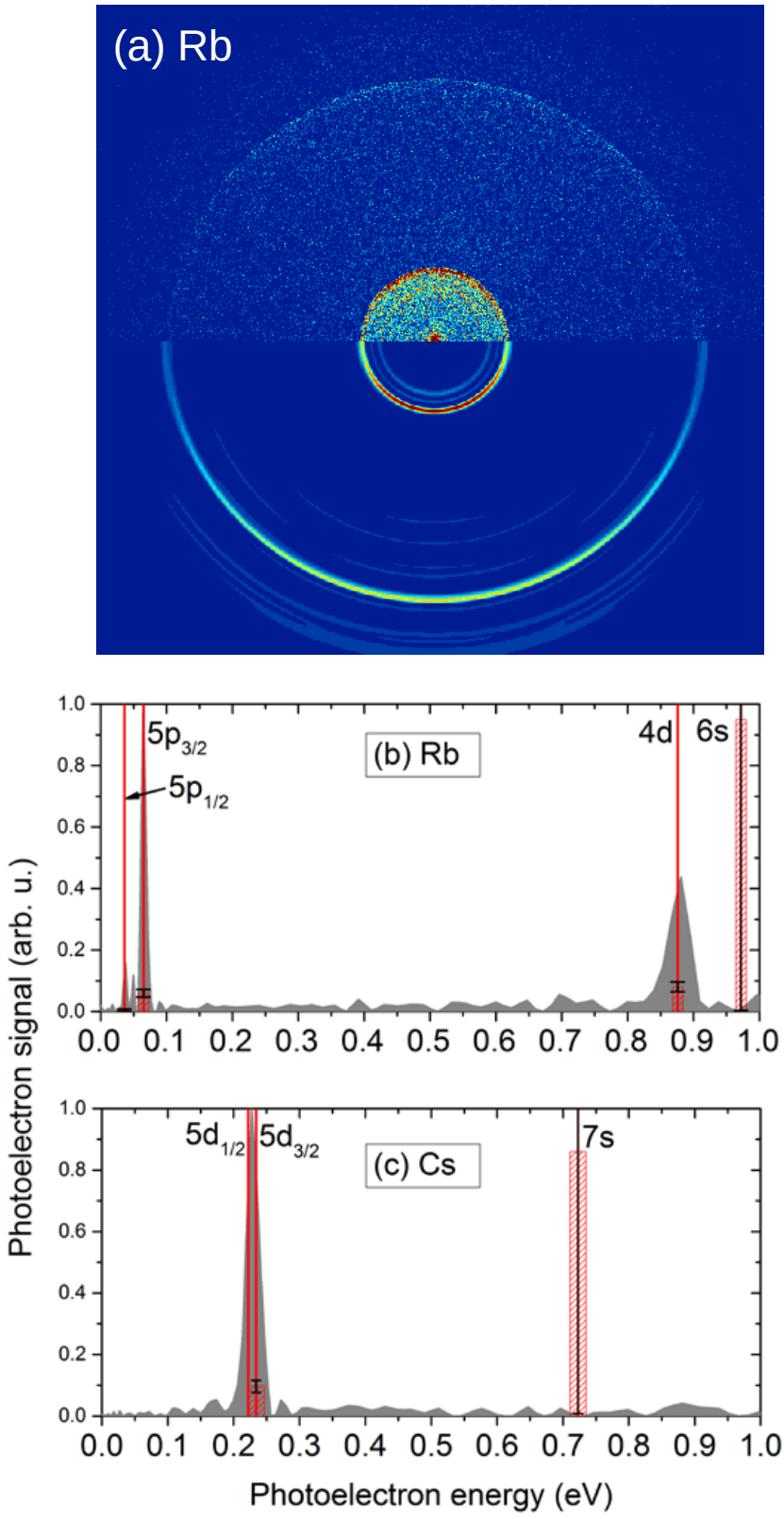

Figure 11: (a) Raw (upper half) and Abel inverted photoelectron image (lower half) of Rb^+ ions recorded with Rb-doped He nanodroplets excited into the $6s\Sigma$ state at the laser wave number $\bar{\nu} = 21\,400$ cm^{-1}. (b) and (c) Photoelectron spectra of Rb and Cs inferred from images recorded at the laser wave numbers 21 400 cm^{-1} and 18 700 cm^{-1}, respectively. The vertical bars represent the relative populations in the respective atomic states.

photon energy for one-photon ionization of the $6p$ states.

This result is at odds with the previous measurements of Li and Na excited to $(n+1)s$ states and to our previous photoelectron spectra recorded at the Rb $6p\Pi$ band where on resonance the dominant photoelectron signals came from the correlating atomic $6p$ state. The lower lying $4d$ and $5p_{3/2,1/2}$ states became particularly apparent for off-resonant excitation. In the present case, however, the absence of the Rb $6s$ and Cs $7s$ photoelectron signals is probably due to the particularly small photoionization cross sections of about 0.01 Mb which result from Cooper minima close to the laser wave numbers used in the experiment.[66,67] For comparison, the detected states have photoionization cross sections > 10 Mb.[67,68]

In the case of Na attached to He nanodroplets, the appearance of lower-lying atomic states was attributed to the short radiative life time of the excited level as compared to the laser pulse length.[36] In the Rb and Cs cases, however, as for the Rb $6p\Pi$ state previously studied,[33] the lifetimes of the free Rb and Cs atoms in the $6s$ and $7s$ states (~ 50 ns[67,69]) by far exceed the laser pulse length (9 ns). Moreover, the appearance of the $4d$ state of Rb and of the $5d$ state of Cs cannot be explained by spontaneous radiative decay due to selection rules. Merely the Rb $5p$ photoelectron signal may contain a contribution from radiative decay. Therefore, we attribute the population of lower-lying electronic states to He droplet-induced relaxation. Whether this relaxation mechanism is predominantly non-radiative or whether the dopant-droplet interaction induces fast radiative decay even at nominally forbidden transitions cannot be determined from theses measurements.

The vertical bars in Fig. 11 (b) and (c) depict the relative populations of the detected states as inferred from the peak integrals weighted by the photoionization cross sections. The corresponding values of the undetected Rb $6s$ and Cs $7s$-states reflect the noise level and can only be considered as upper bounds. Thus, while the populations of the Rb $6s$ and Cs $7s$ states and of the lower lying states (Rb $5s$ and Cs $6s$, $6p$) are undetermined, the Rb $5p_{3/2}$ and $4d$ states are nearly equally populated. When assuming that the Rb $5p$ level is populated purely by radiative decay, this population corresponds to a fraction of about 13% of the original $6s$ population whereas the $5p_{1/2}$ state is populated only by 7%.[69] However, the fact that the measured population of the $5p_{1/2}$ state only

amounts to about 8% of the $5p_{3/2}$ population indicates that an additional droplet-induced decay process is active. In the case of Cs only the $5d$ state is detected so no quantitative comparison with other states can be made.

The detection of photoelectrons exclusively out of relaxed states seems to contradict the results from ion imaging which clearly demonstrate that desorption proceeds according to the pseudo-diatomic model for a fixed $(n+1)s\Sigma$ electronic configuration. For Na excited into the droplet-perturbed states $5s$ and $4d$, the presence of relaxation channels was also observed in the speed distributions of the desorbed atoms.[44] A broad, nearly laser wavelength independent component extending out to velocities $\sim$1500 m/s (kinetic energy $\sim$270 meV) was assigned to atoms having undergone relaxation to the lower $3d$-level. However, in the present experiments on Rb and Cs in the $(n+1)s$-state, no such broad component of the ion distributions is observed (see Fig. 3). The range of kinetic energies observed (Fig. 6) matches well the values expected for dissociation to proceed along the Rb and Cs $(n+1)s\Sigma$ potentials, see Fig. 1.

Furthermore, we have considered the possibility that the photoelectron peaks from relaxed states could be associated with Rb_2^+ and Cs_2^+ dimer ions. However, the relative yield of dimers falls far below the proportion of photoelectrons in relaxed states. Besides, the dependence of the signal intensity of the relaxed electrons on the Rb and Cs vapor pressure in the doping cells clearly indicates that these electrons correlate to Rb^+ and Cs^+ atomic ions. In addition, the possible correlation of these electrons with large ion masses, resulting from unfragmented ion-doped He droplets, was probed by performing dedicated time-of-flight measurements using a different detection unit. The measured proportion of large cluster ions to Rb^+ again stayed well behind that of relaxed electrons to (undetected) electrons out of the Rb $6s$-state. However, due to the uncertainty in determining the relative detection efficiency for large ions, this possibility cannot strictly be ruled out.

Thus, our observations seem to imply that electronic relaxation occurs with some time delay with respect to the strong repulsive interaction which accelerates the dopant atom away from the droplet surface. He induced electronic couplings may be facilitated by the formation of a com-

pressed shell of He atoms around the dopant in the course of desorption (t =0.5-1.5 ps, see Fig. 8). Theoretical modeling of the coupled electron dynamics of excited dopant-droplet complexes as well as time and mass-resolved ion and electron imaging experiments are needed to resolve this puzzling issue.

For the sake of completeness we present in Fig. 12 the results of analyzing a series of photoelectron images taken within the Rb $6s\Sigma$ band. The slight shift to higher wave numbers of the spectral feature measured by detecting electrons with respect to ions [Fig. 12 (a)] likely results from contributions of ionized Rb_2 in the electron measurement.

The relative yields of photoelectrons out of the relaxed states $4d$, $5p_{3/2}$, and $5p_{1/2}$ are depicted in Fig. 12 (b). Similarly to our previous measurements around the Rb $6p\Pi$ state, the relative populations of the lowest detected levels increase as the laser is detuned below the droplet resonance. This change in relative populations likely reflects the variation of the monomer to dimer ratio. Changing relaxation rates into the various target electronic states of Rb due to droplet interactions may also contribute.

The anisotropy parameters β_2 and β_4, which characterize the angular distribution of emitted electrons by two-photon ionization,[70] are depicted in Fig. 12 (c) and (d). The values of β_2 remain nearly constant within the accuracy of the measurement over the excitation spectrum. The β_4 values for the $5p$ states are roughly consistent with zero for all laser wave numbers. This indicates vanishing alignment of the electron orbitals as previously found for Rb $6p\Pi$ excitation.[33] However, the $4d$ orbital appears to retain a certain degree of orbital alignment when exciting on the blue side of the Rb $6s\Sigma$ band. Likely, this is due to faster desorption when exciting further up on the repulsive branch of the Rb-He_N potential.

Summary

We have studied the desorption dynamics of the heavy alkali metal atoms Rb and Cs off the surface of He nanodroplets, initiated by excitation to the perturbed $6s$ and $7s$ states, respectively. As

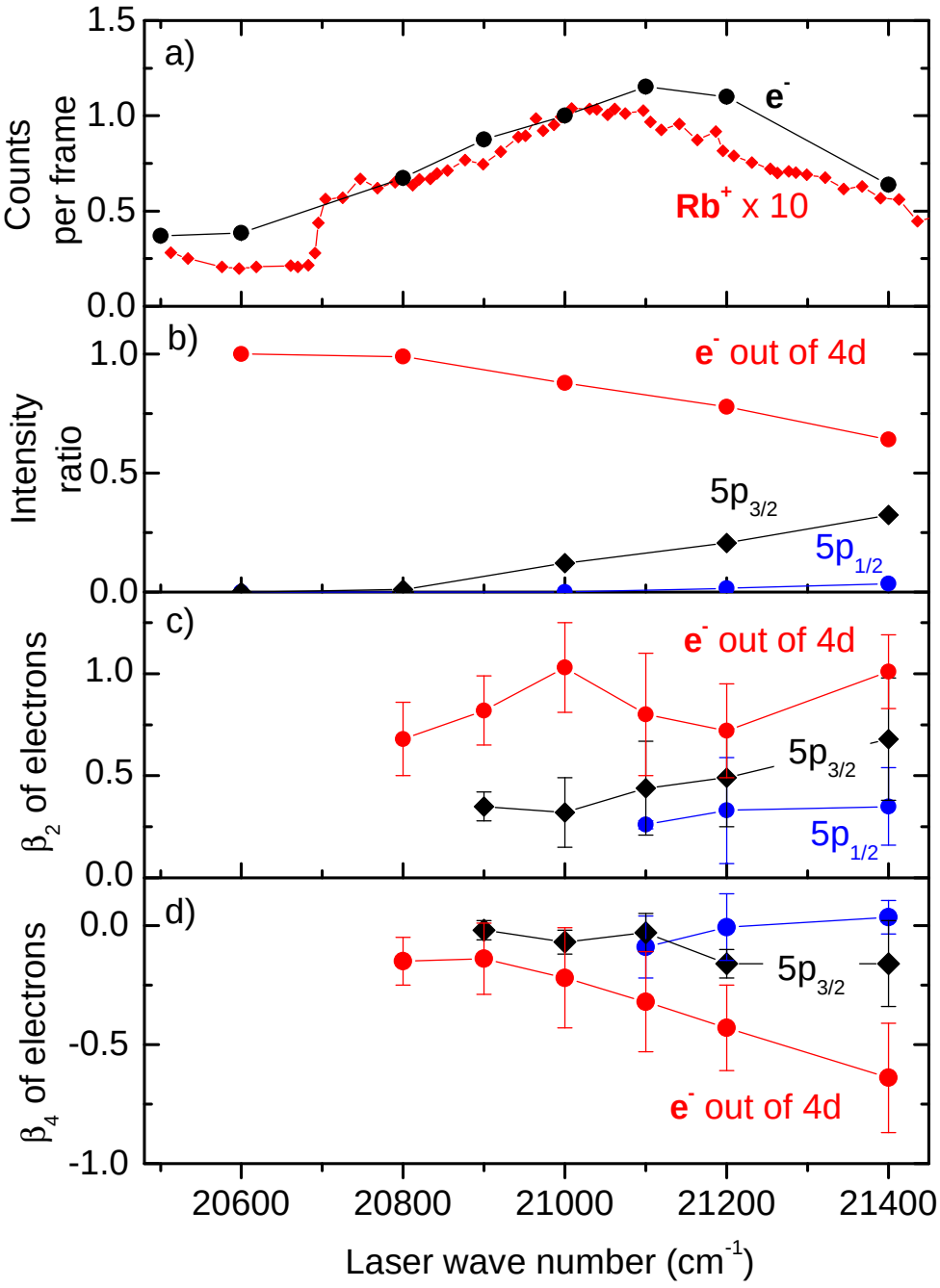

Figure 12: Total photoion signal and photoelectron counts (a), relative abundances of electrons out of different atomic states (b), and anisotropy parameters β_2 (c) and β_4 (d) inferred from electron images recorded a various laser wavelengths around the maximum of the Rb $6s\Sigma$ absorption band.

for Li and Na adatoms,[22] the calculations reveal a complex response of the helium droplet to the impulsive perturbation induced by the excitation of the Rb and Cs adatoms. We find significant local deformations of the droplets and three distinct types of non-linear density waves which propagate through the droplets at different speeds. Nevertheless, both the measured and theoretically calculated mean kinetic energies of the desorbed atoms, which are in excellent agreement, can be modeled as a simple pseudodiatomic direct photodissociation reaction driven by a highly repulsive interaction. We find values of the effective mass of the He droplet interacting with Rb and Cs of about 10 and 13 He atoms, respectively. Deviations from this simple model are found experimentally for the desorption dynamics of Rb on helium droplets excited to the $6p$ state.

The photoelectron spectra measured upon excitation to the perturbed $6s$ and $7s$ states evidence significant electronic relaxation of the desorbed Rb and Cs atoms into lower-lying states, at variance with analogous measurements using the light alkali species Li and Na attached to He droplets. While the ion and electron measurements appear to be contradictory, possible correlations of the observed electrons with other ion signals can largely be ruled out.

This puzzling issue will be further studied by measuring photoelectron spectra with femtosecond time-resolution in pump-probe experiments. Further theoretical work in this direction is also planned.

Acknowledgement

The authors gratefully acknowledge support by DGI, Spain (FEDER) under Grants No. FIS2011-28617-C02-01, by Generalitat de Catalunya (2009SGR1289), and by the Deutsche Forschungsgemeinschaft. AL has been supported by the ME (Spain) FPI program, Grant No. BES-2012-057439.

Animated views (mpeg-files) of the evolution of the helium density distributions upon excitation of rubidium and cesium adatoms are available as Supporting Information. This material is available free of charge via the Internet at http://pubs.acs.org.

References

(1) Stienkemeier, F.; Vilesov, A. F. Electronic spectroscopy in He droplets. *J. Chem. Phys.* **2001**, *115*, 10119–10137.

(2) Toennies, J. P.; Vilesov, A. F. Superfluid helium droplets: A uniquely cold nanomatrix for molecules and molecular complexes. *Angew. Chem. Int. Ed.* **2004**, *43*, 2622–2648.

(3) Stienkemeier, F.; Lehmann, K. K. Spectroscopy and dynamics in helium nanodroplets. *J. Phys. B: At. Mol. Opt. Phys.* **2006**, *39*, R127 – R166.

(4) Barranco, M.; Guardiola, R.; Hernández, S.; Mayol, R.; Navarro, J.; Pi, M. Helium Nanodroplets: an Overview. *J. Low Temp. Phys.* **2006**, *142*, 1–81.

(5) Kornilov, O.; Bünermann, O.; Haxton, D. J.; Leone, S. R.; Neumark, D. M.; Gessner, O. Femtosecond Photoelectron Imaging of Transient Electronic States and Rydberg Atom Emission from Electronically Excited He Droplets. *J. Phys. Chem. A* **2011**, *115*, 7891–7900.

(6) Bünermann, O.; Kornilov, O.; Haxton, D. J.; Leone, S. R.; Neumark, D. M.; Gessner, O. Ultrafast probing of ejection dynamics of Rydberg atoms and molecular fragments from electronically excited helium nanodroplets. *J. Chem. Phys.* **2012**, *137*, 214302.

(7) Droppelmann, G.; Bünermann, O.; Schulz, C. P.; Stienkemeier, F. Formation Times of RbHe Exciplexes on the Surface of Superfluid versus Normal Fluid Helium Nanodroplets. *Phys. Rev. Lett.* **2004**, *93*, 023402.

(8) Döppner, T.; Fennel, T.; Diederich, T.; Tiggesbäumker, J.; Meiwes-Broer, K. H. Controlling the Coulomb Explosion of Silver Clusters by Femtosecond Dual-Pulse Laser Excitation. *Phys. Rev. Lett.* **2005**, *94*, 013401.

(9) Claas, P.; Droppelmann, G.; Schulz, C. P.; Mudrich, M.; Stienkemeier, F. Wave packet dynamics of potassium dimers attached to helium nanodroplets. *J. Phys. B* **2006**, *39*, S1151.

(10) Przystawik, A.; Göde, S.; Döppner, T.; Tiggesbäumker, J.; Meiwes-Broer, K.-H. Light induced collapse of metastable magnesium complexes formed in helium nanodroplets. *Phys. Rev. A* **2008**, *78*, 021202.

(11) Mudrich, M.; Heister, P.; Hippler, T.; Giese, C.; Dulieu, O.; Stienkemeier, F. Spectroscopy of triplet states of Rb_2 by femtosecond pump-probe photoionization of doped helium nanodroplets. *Phys. Rev. A* **2009**, *80*, 042512.

(12) Pentlehner, D.; Nielsen, J. H.; Slenczka, A.; Mølmer, K.; Stapelfeldt, H. Impulsive Laser Induced Alignment of Molecules Dissolved in Helium Nanodroplets. *Phys. Rev. Lett.* **2013**, *110*, 093002.

(13) Pentlehner, D.; Nielsen, J. H.; Christiansen, L.; Slenczka, A.; Stapelfeldt, H. Laser-induced adiabatic alignment of molecules dissolved in helium nanodroplets. *Phys. Rev. A* **2013**, *87*, 063401.

(14) Göde, S.; Irsig, R.; Tiggesbäumker, J.; Meiwes-Broer, K.-H. Time-resolved studies on the collapse of magnesium atom foam in helium nanodroplets. *New J. Phys.* **2013**, *15*, 015026.

(15) Whaley, K. B. Structure and dynamics of quantum clusters. *Int. Rev. Phys. Chem.* **1994**, *13*, 41–84.

(16) Kwon, Y.; Huang, P.; Patel, M. V.; Blume, D.; Whaley, K. B. Quantum solvation and molecular rotations in superfluid helium clusters. *J. Chem. Phys.* **2000**, *113*, 6469–6501.

(17) Chin, S. A.; Krotscheck, E. Systematics of pure and doped ^{4}He clusters. *Phys. Rev. B* **1995**, *52*, 10405–10428.

(18) Krotscheck, E.; Zillich, R. Dynamics of ^{4}He droplets. *J. Chem. Phys.* **2001**, *115*, 10161–10174.

(19) Giacomazzi, L.; Toigo, F.; Ancilotto, F. Dynamics of liquid ^{4}He in confined geometries from time-dependent density functional calculations. *Phys. Rev. B* **2003**, *67*, 104501.

(20) Lehtovaara, L.; Kiljunen, T.; Eloranta, J. Efficient numerical method for simulating static and dynamic properties of superfluid helium. *J. Comput. Phys.* **2004**, *78*, 194.

(21) Mateo, D.; Jin, D.; Barranco, M.; Pi, M. Excited electron-bubble states in superfluid ^{4}He: A time-dependent density functional approach. *J. Chem. Phys.* **2011**, *134*, 044507.

(22) Hernando, A.; Barranco, M.; Pi, M.; Loginov, E.; Langlet, M.; Drabbels, M. Desorption of alkali atoms from ^{4}He nanodroplets. *Phys. Chem. Chem. Phys.* **2012**, *14*, 3996–4010.

(23) Mateo, D.; Hernando, A.; Barranco, M.; Loginov, E.; Drabbels, M.; Pi, M. Translational dynamics of photoexcited atoms in ^{4}He nanodroplets: the case of silver. *Phys. Chem. Chem. Phys.* **2013**, *15*, 18388–18400.

(24) Mateo, D.; Leal, A.; Hernando, A.; Barranco, M.; Pi, M.; Cargnoni, F.; Mella, M.; Zhang, X.; Drabbels, M. Communication: Nucleation of quantized vortex rings in 4He nanodroplets. *J. Chem. Phys.* **2014**, *140*, 131101.

(25) Dalfovo, F. Atomic and molecular impurities in ^{4}He clusters. *Z. Phys. D* **1994**, *29*, 61–66.

(26) Ancilotto, F.; DeToffol, G.; Toigo, F. Sodium dimers on the surface of liquid ^{4}He. *Phys. Rev. B* **1995**, *52*, 16125–16129.

(27) Stienkemeier, F.; Ernst, W. E.; Higgins, J.; Scoles, G. On the use of liquid helium cluster beams for the preparation and spectroscopy of the triplet states of alkli dimers and other weakly bound complexes. *J. Chem. Phys.* **1995**, *102*, 615–617.

(28) Reho, J.; Higgins, J.; Callegari, C.; Lehmann, K. K.; Scoles, G. Alkali-helium exciplex formation on the surface of helium nanodroplets. I. Dispersed emission spectroscopy. *J. Chem. Phys.* **2000**, *113*, 9686–9693.

(29) Schulz, C. P.; Claas, P.; Stienkemeier, F. Formation of K*He exciplexes on the surface of helium nanodroplets studied in real time. *Phys. Rev. Lett.* **2001**, *87*, 153401.

(30) Callegari, C.; Ancilotto, F. Perturbation Method to Calculate the Interaction Potentials and Electronic Excitation Spectra of Atoms in He Nanodroplets. *J. Phys. Chem. A* **2011**, *115*, 6789–6796.

(31) Auböck, G.; Nagl, J.; Callegari, C.; Ernst, W. E. Electron Spin Pumping of Rb Atoms on He Nanodroplets via Nondestructive Optical Excitation. *Phys. Rev. Lett.* **2008**, *101*, 035301.

(32) Theisen, M.; Lackner, F.; Ernst, W. E. Rb and Cs Oligomers in Different Spin Configurations on Helium Nanodroplets. **2011**, *115*, 7005–7009.

(33) Fechner, L.; Grüner, B.; Sieg, A.; Callegari, C.; Ancilotto, F.; Stienkemeier, F.; Mudrich, M. Photoionization and imaging spectroscopy of rubidium atoms attached to helium nanodroplets. *Phys. Chem. Chem. Phys.* **2012**, *14*, 3843 –âĂŞ 3851.

(34) Stienkemeier, F.; Higgins, J.; Callegari, C.; Kanorsky, S. I.; Ernst, W. E.; Scoles, G. Spectroscopy of alkali atoms (Li, Na, K) attached to large helium clusters. *Z. Phys. D* **1996**, *38*, 253–263.

(35) Bünermann, O.; Droppelmann, G.; Hernando, A.; Mayol, R.; Stienkemeier, F. Unraveling the Absorption Spectra of Alkali Metal Atoms Attached to Helium Nanodroplets. *J. Phys. Chem. A* **2007**, *111*, 12684 – 12694.

(36) Loginov, E.; Callegari, C.; Ancilotto, F.; Drabbels, M. Spectroscopy on Rydberg States of Sodium Atoms on the Surface of Helium Nanodroplets. *J. Phys. Chem. A* **2011**, *115*, 6779–6788.

(37) Lackner, F.; Krois, G.; Theisen, M.; Koch, M.; Ernst, W. E. Spectroscopy of nS, nP, and nD Rydberg series of Cs atoms on helium nanodroplets. *Phys. Chem. Chem. Phys.* **2011**, *13*, 18781–18788.

(38) Busch, G. E.; Wilson, K. R. Triatomic Photofragment Spectra. II. Angular Distributions from NO_2 Photodissociation. *J. Chem. Phys.* **1972**, *56*, 3638–3654.

(39) Reho, J.; Callegari, C.; Higgins, J.; Ernst, W. E.; Lehmann, K. K.; Scoles, G. Spin-orbit effects in the formation of the Na-He excimer on the surface of He clusters. *Faraday Discussion* **1997**, *108*, 161–174.

(40) Brühl, F. R.; Trasca, R. A.; Ernst, W. E. Rb–He exciplex formation on helium nanodroplets. *J. Chem. Phys.* **2001**, *115*, 10220–10224.

(41) Mudrich, M.; Droppelmann, G.; Claas, P.; Schulz, C.; Stienkemeier, F. Quantum interference spectroscopy of RbHe exciplexes formed on helium nanodroplets. *Phys. Rev. Lett.* **2008**, *100*, 023401.

(42) Giese, C.; Mullins, T.; Grüner, B.; Weidemüller, M.; Stienkemeier, F.; Mudrich, M. Formation and relaxation of RbHe exciplexes on He nanodroplets studied by femtosecond pump and picosecond probe spectroscopy. *J. Chem. Phys.* **2012**, *137*, 244307.

(43) Takahashi, Y.; Sano, K.; Kinoshita, T.; Yabuzaki, T. Spectroscopy of alkali atoms and molecules in superfluid helium. *Phys. Rev. Lett.* **1993**, *71*, 1035–1038.

(44) Loginov, E.; Drabbels, M. Dynamics of Excited Sodium Atoms Attached to Helium Nanodroplets. *J. Phys. Chem. A* **2014**, *118*, 2738–2748.

(45) Loginov, E.; Drabbels, M. Spectroscopy and dynamics of barium-doped helium nanodroplets. *J. Chem. Phys.* **2012**, *136*, 154302.

(46) Loginov, E.; Drabbels, M. Excited State Dynamics of Ag Atoms in Helium NanodropletsâĂă. *J. Phys. Chem. A* **2007**, *111*, 7504–7515.

(47) Kautsch, A.; Koch, M.; Ernst, W. E. Electronic Relaxation after Resonant Laser Excitation of Cr in Superfluid Helium Nanodroplets. *J. Phys. Chem. A* **2013**, *117*, 9621–9625.

(48) Lindebner, F.; Kautsch, A.; Koch, M.; Ernst, W. E. Laser ionization and spectroscopy of Cu in superfluid helium nanodroplets. *Int. J. Mass Spectrom.* **2014**, *365 - 366*, 255 – 259.

(49) Vrakking, M. J. J. An iterative procedure for the inversion of two-dimensional ion/photoelectron imaging experiments. *Rev. Sci. Instr.* **2001**, *72*, 4084.

(50) Garcia, G. A.; Nahon, L.; Powis, I. Two-dimensional charged particle image inversion using a polar basis function expansion. *Rev. Sci. Instrum.* **2004**, *75*, 4989–4996.

(51) Ellison, F. O. A Method of Diatomics in Molecules. I. General Theory and Application to H_2O. *J. Am. Chem. Soc.* **1963**, *85*, 3540.

(52) Dalfovo, F.; Lastri, A.; Pricaupenko, L.; Stringari, S.; Treiner, J. Structural and dynamical properties of superfluid helium. *Phys. Rev. B* **1995**, *52*, 1193.

(53) Patil, S. H. Adiabatic potentials for alkali-inert gas systems in the ground state. *J. Chem. Phys.* **1991**, *94*, 8089–8095.

(54) Pascale, J. Use of *l*-dependent preudopotemtials in the study of alkali-metal-atom-He systems. The adiabatic molecular potentials. *Phys. Rev. A* **1983**, *28*, 632–644.

(55) Ralston, A.; Wilf, H. S. *Mathematical methods for digital computers*; John Wiley and Sons, New York, 1960.

(56) Koutselos, A. D.; Mason, E. A.; Viehland, L. A. Interaction universality and scaling laws for interaction potentials between closedâĂŘshell atoms and ions. *J. Chem. Phys.* **1990**, *93*, 7125–7136.

(57) LeRoy, R. J.; Kraemer, G. T. BCONT 2.2. Computer Program for Calculating Absorption Coefficients, Emission Intensities or (Golden Rule) Predissociation Rates. The source code and manual for this program may be obtained from "Computer ProgramsÂt'Ât' link at http://leroy.uwaterloo.ca. University of Waterloo Chemical Physics Research Report CP-650R^2, 2004.

(58) Mateo, D.; Hernando, A.; Barranco, M.; Mayol, R.; Pi, M. Absorption spectrum of atomic impurities in isotopic mixtures of liquid helium. *Phys. Rev. B* **2011**, *83*, 174505.

(59) Pifrader, A.; Allard, O.; Auböck, G.; Callegari, C.; Ernst, W. E.; Huber, R.; Ancilotto, F. One- and two-photon spectroscopy of highly excited states of alkali-metal atoms on helium nanodroplets. *J. Chem. Phys.* **2010**, *133*, 164502.

(60) Lozeille, J.; Fioretti, A.; Gabbanini, C.; Huang, Y.; Pechkis, H.; Wang, D.; Gould, P.; Eyler, E.; Stwalley, W.; Aymar, M.; Dulieu, O. Detection by two-photon ionization and magnetic trapping of cold Rb_2 triplet state molecules. *Eur. Phys. J. D* **2006**, *39*, 261 –âĂŞ 269.

(61) Zare, R. N. Photoejection Dynamics. *Mol. Photochem.* **1972**, *44*, 1.

(62) Ancilotto, F.; Cheng, E.; Cole, M. W.; Toigo, F. The binding of alkali atoms to the surfaces of liquid helium and hydrogen. *Z. Phys. D* **1995**, *98*, 323–329.

(63) Gallagher, T. *Rydberg Atoms*; Cambridge University Press: Cambridge, U.K., 1994.

(64) Peterka, D. S.; Kim, J. H.; Wang, C. C.; Poisson, L.; Neumark, D. M. Photoionization Dynamics of Pure Helium Droplets. *J. Phys. Chem. A* **2007**, *111*, 7449 – 7459.

(65) Loginov, E. Photoexcitation and Photoionization Dynamics of Doped Liquid Helium-4 Nanodroplets. Ph.D. thesis, École Polytechnique Fédérale de Lausanne, 2008.

(66) Moskvin, Y. V. Photoionization of atoms and recombination of ions in the vapors of alkali metals. *Opt. Spectrosc.* **1963**, *15*, 316 – 318.

(67) Lahiri, J.; Manson, S. T. Oscillator-strength distributions for discrete and continuum transitions of excited states of cesium. *Phys. Rev. A* **1986**, *33*, 3151–3165.

(68) Aymar, M.; Robaux, O.; Wane, S. Central-field calculations of photoionisation cross sections of excited states of Rb and Sr^+ and analysis of photoionisation cross sections of excited alkali atoms using quantum defect theory. *J. Phys. B* **1984**, *17*, 993 – 1007.

(69) Heavens, O. Radiative Transition Probabilities of the Lower Excited States of the Alkai Metals. *J. Opt. Soc. Am.* **1961**, *51*, 1058–1061.

(70) Reid, K. L. Photoelectron angular distributions. *Annu. Rev. Phys. Chem.* **2003**, *54*, 397 âĂŞ 424.

Table 1: Characteristics of the experimental and theoretical kinetic energy distributions of the desorbed alkali atoms, see text for details. All masses are given in amu.

Ak	m_{Ak} (exp)	η (exp)	η (th)	m_{eff} (exp)	m_{eff} (th)	$\langle r_e \rangle$ (Å)	m_{ef}
Li	6.94	0.687	0.756	15.2	21.5	5.35	
Na	23.0	0.516	0.583	24.6	32.2	5.55	
Rb	85.5	0.327	0.324	41.9	41.0	6.54	
Cs	132.9	0.281	0.273	51.8	50.5	6.78	